Ninth International Conference on
THIN-WALLED STRUCTURES – ICTWS2023
Sydney, Australia, Nov 29 – Dec 1, 2023

TESTS ON COLD-FORMED STAINLESS STEEL BUILT-UP BOX SECTION STUB COLUMNS

Hai-Ting Li*, Chun-Chi Jin*, Qiu-Yun Li and Ben Young****

*Department of Civil Engineering, Shanghai Jiao Tong University, Shanghai, China
e-mails: haiting.li@sjtu.edu.cn, jincc03@sjtu.edu.cn
**Department of Civil and Environmental Engineering, The Hong Kong Polytechnic University, Hong Kong, China
e-mails: qiuyun.li@polyu.edu.hk, ben.young@polyu.edu.hk

Keywords: Built-up section; Cold-formed; Direct strength method; Stainless steel; Stub column

Abstract. *A test program is presented in this paper to investigate the behavior of cold-formed stainless steel built-up box section stub columns. Three types of built-up box sectional configurations were composed by connecting two unlipped channels, two lipped channels as well as one unlipped channel and one lipped channel at the flanges using self-plugging rivets. The unlipped and lipped channel components were brake-pressed from high-strength austenitic stainless steel thin sheets. A total of 13 stub columns were tested to cover four series of overall web height-to-plate thickness ratio. The experimental results in terms of failure mode, load versus axial shortening response and ultimate capacity were obtained for all the test specimens. Moreover, by comparing the experimental ultimate capacities with nominal (unfactored) strengths, the applicability of design provisions provided in the ASCE/SEI 8-22 specification was assessed for cold-formed stainless steel built-up sections under compression. It is found that the codified design rules generally resulted in unconservative strength predictions for the high-strength austenitic stainless steel built-up box section stub columns.*

1 INTRODUCTION

Recent decades have witnessed the increasingly utilization of stainless steel in various architectural and structural applications due to its beneficial merits such as aesthetic appearance, remarkable corrosion resistance and low life-cycle costs [1-3]. Stainless steel is more expensive than traditional carbon steel. To minimize material costs, cold-formed stainless steel (CFSS) members with superior strength-to-weight ratio are desirably used in practice. With the growing demands for high structural efficiency of cold-formed members, the advanced configuration of built-up sections has been emerged by composing several individual sections utilizing discrete connectors [4-8]. Compared to single section counterparts, the structural behavior of CFSS members with built-up sections could be more complex as a result of discretely distributed fasteners along the member length. However, up to now, research studies on CFSS built-up section members under axial compression are still limited, especially for CFSS built-up box sections.

To this end, a test program was conducted to examine the performance of cold-formed high-strength austenitic stainless steel built-up box section stub columns. Three types of built-up sectional configurations and four series of overall web height-to-plate thickness ratio were considered. Self-plugging rivets were employed to assemble the built-up box section specimens. Tensile coupon tests were carried out to determine the actual material properties of the CFSS members. In addition, 13 stub columns were tested to obtain failure modes, responses of load versus axial shortening and ultimate capacities. Underpinned by the stub column test results, the appropriateness of design rules as stipulated in the recently updated American Specification ASCE/SEI 8-22 [9] was evaluated for cold-formed high-strength austenitic stainless steel built-up sections under axial compression.

2 TEST PROGRAM

2.1 Test specimens and material properties

In this test program, the unlipped and lipped channels were brake-pressed from stainless steel thin sheets of high-strength austenitic grade QN1803 that employs a new metallurgical technology [10]. Two nominal plate thicknesses (t) of 1.5 and 2.0 mm as well as two nominal overall web heights (H_w) of 100 and 120 mm were devised to constitute four series of channel sections, denoted as S1, S2, S3 and S4, which had the nominal values of overall web height-to-plate thickness ratio (H_w/t) equal to 50, 60, 67 and 80, respectively. As exhibited in Figure 1, three types of built-up sectional configurations composed by connecting two unlipped channels, one lipped channel and one unlipped channel, as well as two lipped channels at the flanges using self-plugging rivets, referred to as UU-, CU- and CC-sections, respectively. The nominal specimen length (L) of 300 or 360 mm was adopted for the UU-, CU- and CC-section stub columns, which was equivalent to three times the nominal overall web height (H_w) of the channel components. Self-plugging rivets with nominal shank diameter and length of 4.8 and 10 mm, respectively, were employed in the test program to assemble the CFSS built-up box section specimens. An intermediate fastener spacing of 100 mm that fulfilled the provision as prescribed in Clause 9.1.2 of the ASCE/SEI 8-22 [9] was utilized along the longitudinal direction of the UU-, CU- and CC-section stub columns, whereas the finer rivet spacings of 50 and 40 mm were arranged at both ends of the specimens with nominal member lengths of 300 and 360 mm, respectively.

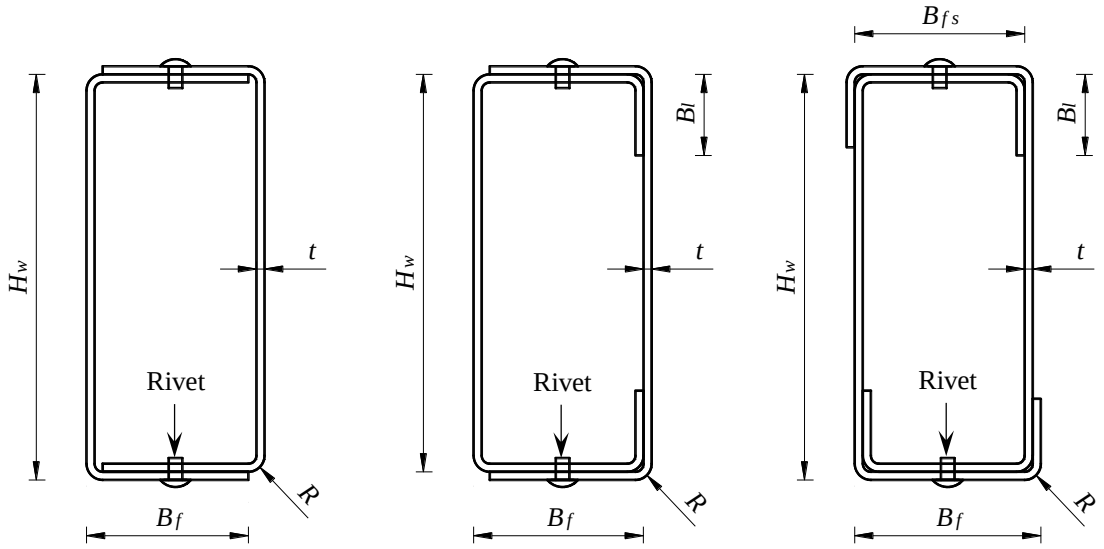

(a) UU-section (b) CU-section (c) CC-section

Figure 1: Configurations and symbol definition of built-up box sections.

In total, 13 stub column tests were carried out on the high-strength austenitic stainless steel built-up sections, covering three built-up box sectional configurations (i.e., UU-, CU- and CC-sections) and four nominal values of overall web height-to-plate thickness ratio (i.e., H_w/t of 50, 60, 67 and 80). The dimension measurements were performed for individual channel components (designated as parts "a" and "b") of all the CFSS built-up box section stub columns before connecting by self-plugging rivets, as reported in Table 1. It should be noted that the nominal flange widths of channel components composing the CC-section specimens had a difference of 2t to facilitate the assembly, as B_f and B_{fs} shown in Figure 1, where t is the plate thickness. The labels of the test specimens were defined to display the information of stainless steel type, built-up sectional configuration and sectional series in sequence. For instance, the

label "HA-CU-S3R" represents the high-strength austenitic (HA) stainless steel stub column specimen with built-up CU-section and nominal overall web height-to-plate thickness ratio of 67 (sectional series S3). The letter "R" at the end of the label indicates that the specimen was loaded as a repeated test.

Table 1: Measured dimensions of high-strength austenitic stainless steel built-up section stub columns.

Specimen	Part	H_w (mm)	B_f (mm)	B_{fs} (mm)	B_l (mm)	t (mm)	R (mm)
HA-UU-S1	a (U)	100.3	40.0	-	-	1.966	3.75
	b (U)	100.1	40.1	-	-	1.972	3.75
HA-UU-S2	a (U)	120.3	40.0	-	-	1.959	3.75
	b (U)	120.1	40.3	-	-	1.973	3.75
HA-UU-S3	a (U)	100.5	40.1	-	-	1.398	3.25
	b (U)	100.6	40.2	-	-	1.410	3.25
HA-UU-S4	a (U)	120.7	40.1	-	-	1.402	3.25
	b (U)	120.9	40.1	-	-	1.398	3.25
HA-CU-S1	a (C)	98.1	41.8	-	20.0	1.963	3.75
	b (U)	102.2	40.1	-	-	1.964	3.75
HA-CU-S2	a (C)	118.6	41.9	-	19.9	1.973	3.75
	b (U)	122.2	40.0	-	-	1.975	3.75
HA-CU-S3	a (C)	99.1	41.7	-	20.1	1.403	3.25
	b (U)	102.2	40.1	-	-	1.397	3.25
HA-CU-S3R	a (C)	99.2	41.8	-	20.0	1.402	3.25
	b (U)	102.5	40.3	-	-	1.403	3.25
HA-CU-S4	a (C)	119.0	41.7	-	19.9	1.399	3.25
	b (U)	122.1	40.1	-	-	1.400	3.25
HA-CC-S1	a (C)	100.1	46.1	41.8	20.0	1.988	3.75
	b (C)	100.2	46.2	41.6	20.0	1.962	3.75
HA-CC-S2	a (C)	119.9	46.1	41.6	20.1	1.968	3.75
	b (C)	120.0	46.1	41.6	20.1	1.959	3.75
HA-CC-S3	a (C)	100.5	45.7	41.3	20.0	1.392	3.25
	b (C)	100.2	45.4	41.3	20.0	1.406	3.25
HA-CC-S4	a (C)	120.8	45.3	41.4	19.9	1.400	3.25
	b (C)	120.5	45.4	41.3	19.9	1.401	3.25

Table 2: Material properties measured from tensile coupon tests.

Coupon type	Specimen	E (GPa)	$\sigma_{0.2}$ (MPa)	σ_u (MPa)	ε_f (%)
Flat	HA-1.5F	190.4	361.6	746.8	60.1
	HA-2.0F	202.3	352.9	737.2	64.7
Corner	HA-1.5C	199.2	600.9	880.2	28.7
	HA-2.0C	205.5	638.2	958.2	38.4

In order to determine the actual material properties of the CFSS stub columns on high-strength austenitic grade QN1803, a series of tensile coupon tests were carried out. Both flat and corner coupon specimens were longitudinally extracted from the representative channel components with nominal plate thicknesses of 1.5 and 2.0 mm. For the flat coupon specimens, the nominal dimensions of 50 mm gauge length and 12.5 mm gauge width were utilized in accordance with recommendations in the ASTM E8/E8M-21 [11]. Referring to the previous studies [12-14], the corner coupon specimens had nominal gauge length and width of 25 and 4 mm, respectively. Based on the static stress-strain relationships obtained from the flat and corner coupon tests, the material properties of Young's modulus (E), 0.2% proof stress ($\sigma_{0.2}$), ultimate tensile strength (σ_u) and strain at facture (ε_f) were determined and are summarized in Table 2, in which the coupon specimens were labelled to identify the particulars of stainless steel type, nominal plate thickness and extraction portion. For example, the label "HA-2.0C"

denotes that the coupon specimen was extracted from the high-strength austenitic (HA) stainless steel channel with nominal plate thickness of 2.0 mm at the corner portion.

2.2 Initial geometric imperfection measurements

Initial local imperfection measurements were performed on the 4 representative specimens HA-CU-S1, HA-CU-S2, HA-CU-S3 and HA-CU-S4 before the stub column tests. For each representative specimen, the initial local imperfections were measured on the webs of both channel components using a digital dial gauge with accuracy of 0.001 mm. To exclude the influence of end cutting, the measurements along the member length were started and terminated at locations 50 mm away from the ends of each specimen. The geometric imperfections were deemed to be zero and maximum at the corner and middle portions of the CFSS sections, respectively. Under this assumption, along the sectional direction, readings of the digital dial gauge were obtained for each measuring surface (i.e., Face A or B shown in Figure 2) at three points, namely two points near the junctions of the web with adjacent flanges and one at the middle of the web. Subsequently, the datum line was established based on the data measured at the two junction points, and the deviation of the measurement at the middle point from the datum line was taken as the value of initial local imperfection (ω_l). The measured distributions of initial local imperfections (ω_l) are displayed in Figure 2 for the representative specimens HA-CU-S1 and HA-CU-S2, where z denotes the longitudinal distance between the measuring location and the measurement start location, and L_m is the longitudinal distance between the measurement start and termination locations. It is noteworthy that the values of ω_l were identified as positive and negative in this study when the measuring surface exhibited convex and concave shapes, respectively. For each representative specimen, the largest absolute value of ω_l obtained from the webs of both channel components was regarded as the magnitude of initial local imperfections, as reported in Figure 2.

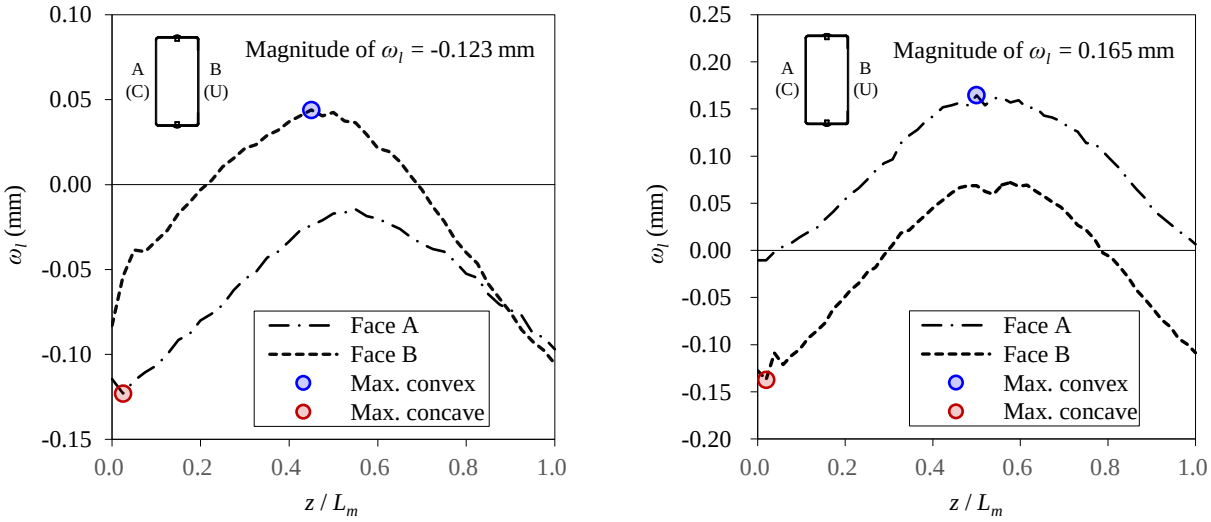

(a) Specimen HA-CU-S1 (b) Specimen HA-CU-S2

Figure 2: Measured distributions of initial local imperfections along the member length.

2.3 Test rig and operation

In this experimental program, the CFSS built-up box section stub columns were tested under fixed-ended boundary conditions. The arrangement of stub column test rig is shown in Figure 3. Before the installation, both ends of the specimens were milled flat to ensure uniform contact between the stub columns and bearing plates. In order to prevent premature failure due to stress concentration, a pair of stiffening devices with a height of 30 mm was clamped to the two ends

of the specimens. A special ball bearing was fastened to the top loading platform, which could freely rotate at the pre-loading stage to eliminate any possible gaps in the setup. Prior to the testing, the special ball bearing was fully locked by four bolts to cater for the fixed-ended boundary condition. The alignment of each stub column was carefully adjusted according to the readings of strain gauges that were affixed onto the outer fibers of the built-up section at mid-length of the member. Additionally, four vertical linear variable displacement transducers (LVDTs) were symmetrically installed at the top loading platform, the average readings of which were utilized to determine the axial shortening of the test specimens. A hydraulic testing machine was adopted to conduct the stub column tests using a loading speed of 0.2 mm/min. During the tests, the readings of strain gauges, LVDTs and applied load were collected at regular time intervals.

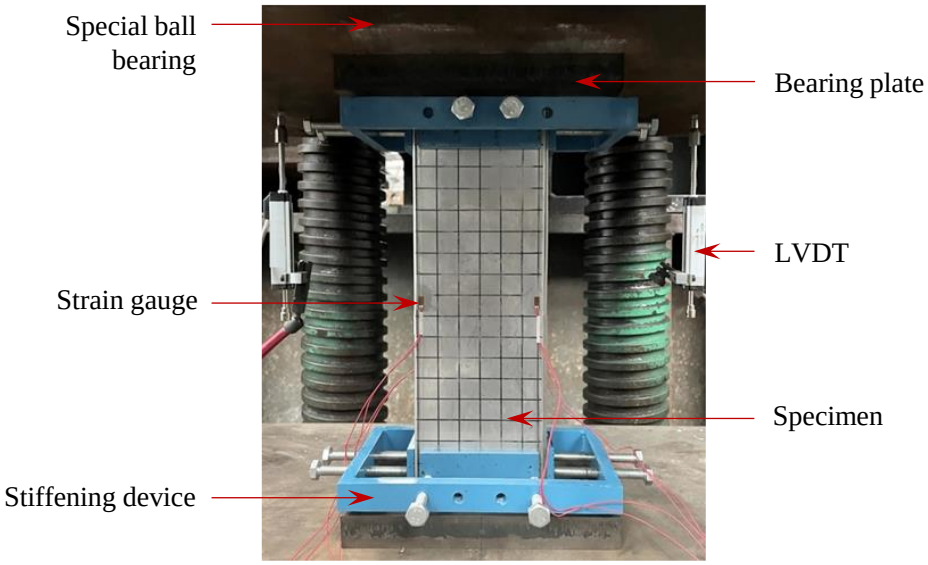

Figure 3: Arrangement of CFSS built-up section stub column test rig.

2.4 Experimental results

The failure modes were observed for the CFSS built-up box section stub columns at the ultimate loads. All the 13 UU-, CU- and CC-section specimens failed by local buckling only and the loosening or failure of self-plugging rivets was not found for any specimens. The local buckling half-waves were visibly observed for the stub columns before reaching the ultimate loads. Generally, near the mid-length of the members, the webs and flanges of the built-up box sections buckled outward and inward, respectively, as exemplified in Figure 4.

The responses of load versus axial shortening are depicted in Figure 5. It was revealed that the load-axial shortening curve of the repeated test specimen HA-CU-S3R almost coincided with that of the specimen HA-CU-S3 with minor discrepancies in both stiffness and ultimate loads. This indicates that the results obtained in this test program were repeatable and reliable. In addition, regarding the load versus axial shortening responses presented in Figure 5, the stub columns with nominal plate thickness of 2.0 mm (i.e., sectional series S1 and S2) normally exhibited greater initial stiffness compared to the specimens with nominal plate thickness of 1.5 mm (i.e., sectional series S3 and S4), which is theoretically related to EA/L, where E is Young's modulus of the material, A denotes the sectional area, and L represents the member length. For the built-up UU-sections consisting of two unlipped channels, the specimens with larger values of H_w/t ratio generally performed better in the post-ultimate stage, as evidenced by the load-axial shortening curves shown in Figure 5(a), where the stub columns with sectional series S1 and S3 display more rapid descent after the ultimate loads relative to those with

sectional series S2 and S4, respectively. However, for the built-up CU- and CC-sections composed by components including at least one lipped channel, the post-ultimate behavior of the stub columns with varying values of H_w/t ratio did not show noticeable differences, as demonstrated in Figure 5(b).

Figure 4: Failure mode of stub column specimen HA-CC-S4.

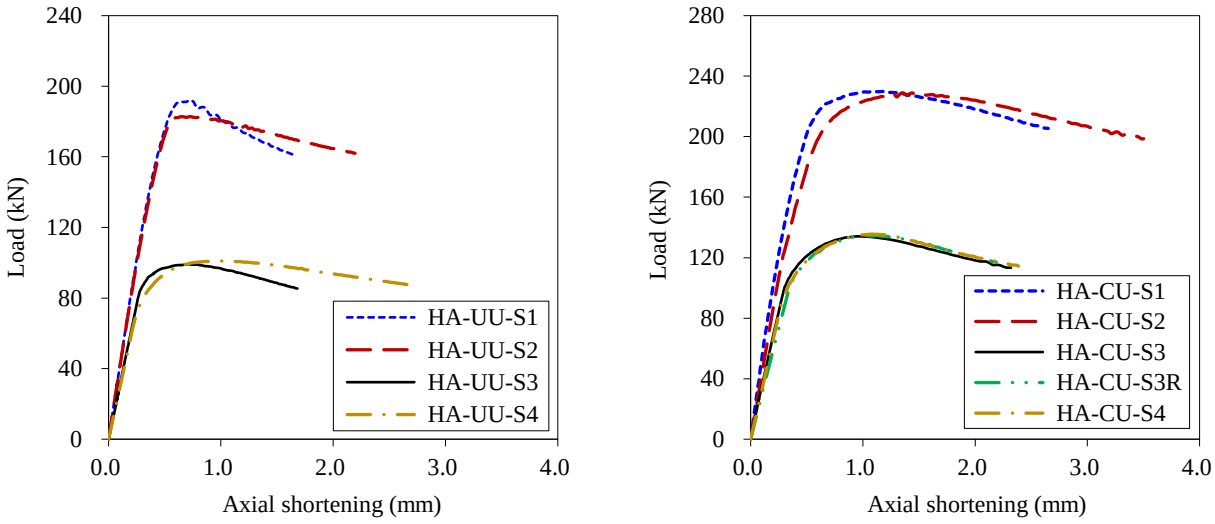

(a) Series HA-UU (b) Series HA-CU

Figure 5: Responses of load versus axial shortening.

The experimental results in terms of failure mode and ultimate capacity (P_{Exp}) are reported in Table 3 for the high-strength austenitic stainless steel stub columns. The normalized loading capacities (P_{Exp}/P_y) of the test specimens with varying H_w/t ratio values are compared in Figure 6, where P_y denotes the yield load of the gross cross-section that was calculated based on the 0.2% proof stress ($\sigma_{0.2}$) measured from the flat portion of the section. As shown in Figure 6, for the same built-up box sectional configurations (i.e., UU-, CU- or CC-sections), the P_{Exp}/P_y values of the stub columns normally decreased with the increase of overall web height-to-plate thickness ratio. On the other hand, for identical nominal values of H_w/t ratio, the test specimens with UU- and CC-sections exhibited the smallest and greatest normalized loading capacities, respectively, which manifested that the built-up CC-sections composed by two

lipped channels outperformed in retarding local buckling than the UU-sections assembled by two unlipped channels. It was revealed that, with the values of H_w/t ratio changing from 50 to 80, the normalized loading capacities (P_{Exp}/P_y) of the high-strength austenitic stainless steel CC-section test specimens were enhanced by 20.8% to 40.6% compared to those of the UU-section counterparts.

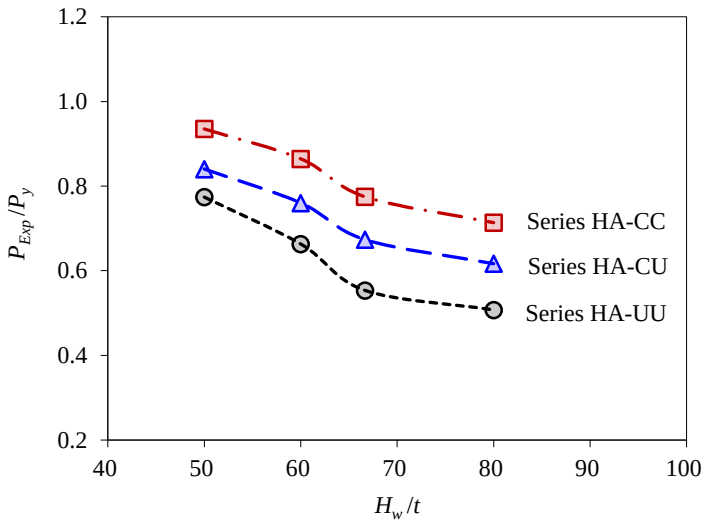

Figure 6: Variations in normalized loading capacity with overall web height-to-plate thickness ratio.

Table 3: Experimental results and comparison with strength predictions.

Specimen	Failure mode	P_{Exp} (kN)	$\frac{P_{Exp}}{P_y}$	P_{ASCE} (kN)	$\frac{P_{Exp}}{P_{ASCE}}$
HA-UU-S1	L	192.1	0.77	255.3	0.75
HA-UU-S2	L	182.8	0.66	236.4	0.77
HA-UU-S3	L	99.2	0.55	136.2	0.73
HA-UU-S4	L	101.0	0.51	124.6	0.81
HA-CU-S1	L	230.1	0.84	282.7	0.81
HA-CU-S2	L	229.3	0.76	260.4	0.88
HA-CU-S3	L	134.2	0.67	151.5	0.89
HA-CU-S3R	L	134.7	0.67	151.2	0.89
HA-CU-S4	L	135.6	0.62	137.8	0.98
HA-CC-S1	L	285.5	0.94	321.6	0.89
HA-CC-S2	L	288.0	0.86	292.8	0.98
HA-CC-S3	L	171.4	0.77	171.0	1.00
HA-CC-S4	L	172.2	0.71	153.9	1.12
Mean (P_m)					0.89
COV (V_P)					0.128
Resistance factor (ϕ)					0.90
Reliability index (β)					2.24

Note: L = local buckling.

3 ASSESSMENT OF CURRENT DESIGN RULES

3.1 General

A new edition of the American Specification ASCE/SEI 8-22 [9] has been published recently to include significant advancements in the research knowledge on cold-formed stainless steel structural members over the past two decades [15]. For the design of CFSS members under axial compression, the updated strength curves such as global buckling curves proposed by Arrayago and Rasmussen [16] as well as direct strength method (DSM) curves of local buckling and distortional buckling recommended by Becque et al. [17] are adopted in the ASCE/SEI 8-

22 [9]. It is worth noting that these updated strength curves are semi-empirical and were calibrated against the existing experimental and numerical data on CFSS columns with limited types of cross-sectional profiles including unlipped channel sections, lipped channel sections and built-up I-sections. Therefore, ultimate capacities obtained from the stub column tests were compared with nominal (unfactored) axial strengths to assess the applicability of the design rules based on DSM as per the ASCE/SEI 8-22 [9] for cold-formed high-strength austenitic stainless steel built-up box sections under compression.

Moreover, the statistical analysis method in Chapter 11 of the ASCE/SEI 8-22 [9] was utilized to evaluate the reliability of the codified design provisions for the CFSS built-up box section stub columns. The target value of reliability index (β) equal to 2.5 and a resistance factor (ϕ) of 0.90 were employed in the reliability analysis. Referring to Tables 11-1 and 11-2 of the ASCE/SEI 8-22 [9], the mean values of material and fabrication factors were taken as M_m=1.25 and F_m=1.0 for the high-strength austenitic stainless steel structural members with the corresponding coefficients of variation (COVs) of V_M=0.10 and V_F=0.05, respectively. A governing dead load (DL) and live load (LL) combination of 1.2DL+1.6LL with a dead-to-live load ratio of 1/5 was adopted to compute the COV of load effect. In order to account for the number of experimental data, a correction factor (C_P) calculated from Eq. 11-4 of the ASCE/SEI 8-22 [9] was used in the determination of reliability index.

3.2 Elastic buckling analysis

For CFSS members under compression, critical elastic buckling loads are key parameters in predicting axial strengths in accordance with the DSM codified in the ASCE/SEI 8-22 [9]. The advanced finite strip analysis program CUFSM [18] was adopted in this study to determine the critical elastic loads of cross-sectional instabilities, namely local buckling and distortional buckling, if possible to occur. Finite strip methods essentially discretize thin-walled members into series of uniformly longitudinal strips along the sectional direction [19]. Hence, the discontinuity along the longitudinal direction of members caused by discrete fasteners cannot be perfectly simulated using CUFSM [18]. For the built-up UU-, CU- and CC-sections, the solid blocks model, as adopted in the previous research [20, 21], was utilized in this study to account for the presence of self-plugging rivets in the finite strip analysis. More specifically, in the CUFSM [18], two channels of each built-up section were connected by the elastic deformation solid blocks that located at the actual positions of self-plugging rivets and possessed the width equivalent to the nominal diameter of rivets.

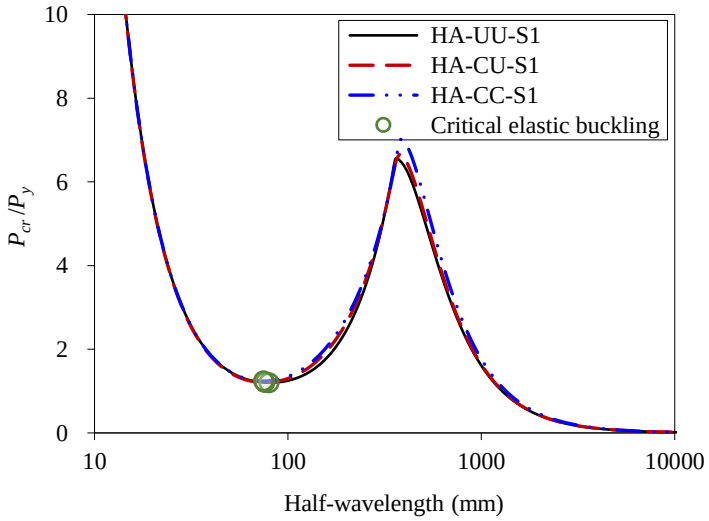

Figure 7: Signature curves of typical UU-, CU- and CC-sections.

Figure 7 displays the signature curves of typical UU-, CU- and CC-sections with nominal overall web height-to-plate thickness ratio (H_w/t) of 50. Only one critical elastic buckling load (minimum value) corresponding to cross-sectional instability was found on the signature curves for the three types of built-up box sections under axial compression, at which the local buckling of the webs was identified. Based on the solid blocks model, the signature curves and obtained P_{crl}/P_y values of the UU-, CU- and CC-sections with identical H_w/t ratio were fairly similar, as shown in Figure 7, where P_{crl} denotes the critical elastic local buckling load.

3.3 Design rules of ASCE/SEI 8-22

According to the results of elastic buckling analysis presented in Section 3.2 of this paper, the cross-sectional instability of the UU-, CU- and CC-sections under axial compression merely involved local buckling. Hence, the nominal axial strengths (P_n) of the CFSS built-up box section columns were determined from Eq. (1), where P_{ne} is the nominal axial strength for yielding and global buckling, and P_{nl} is the nominal axial strength for local buckling interacting with yielding and global buckling.

$$P_n = \min\left(P_{ne}, P_{nl}\right) \tag{1}$$

As specified in Clause 5.2 of the ASCE/SEI 8-22 [9], the value of P_{ne} could be computed in accordance with Eqs. (2) and (3), in which $\lambda_c = \sqrt{F_y/F_{cre}}$; F_y and F_u represent the yield and ultimate stresses of the material, respectively, and A_g denotes the area of the gross cross-section; α, β_0, β_1 and β_2 are the global buckling coefficients that are prescribed as 1.13, 0.24, 0.41 and 0.69, respectively, in Table 5-1 of the American Specification [9] for austenitic stainless steel. As expected that the CFSS built-up box section columns did not fail by torsional buckling nor flexural-torsional buckling, the critical elastic flexural buckling stresses (F_{cre}) were calculated from Eq. 5-6 of the ASCE/SEI 8-22 [9]. In addition, the direct strength method (DSM) to predict the nominal axial strengths (P_{nl}) of CFSS columns subjected to local buckling interacting with yielding and global buckling is provided in Clause 5.3 of the ASCE/SEI 8-22 [9]. The codified DSM curve for the determination of P_{nl} is expressed in Eq. (4), which was derived by Becque et al. [17] for stainless steel compression members and calibrated against the experimental and numerical data covering lipped channel sections as well as built-up I-sections. In Eq. (4), $\lambda_l = \sqrt{P_{ne}/P_{crl}}$ and P_{crl} denotes the critical elastic local buckling load. The DSM formula of Eq. (4) was adopted to compute P_{nl} for the high-strength austenitic stainless steel built-up box section stub columns based on P_{crl} obtained from the approach presented in Section 3.2 of this paper.

$$P_{ne} = A_g F_n \tag{2}$$

$$F_n = \begin{cases} F_y + \left(1 - \frac{\lambda_c}{\beta_0}\right)\left(F_u - F_y\right) & \text{for } \lambda_c \le \beta_0 \\ 1.2\left(\beta_1^{\lambda_c^{\alpha}}\right) F_y & \text{for } \beta_0 < \lambda_c \le 1.8 \\ \beta_2 F_{cre} & \text{for } \lambda_c > 1.8 \end{cases} \tag{3}$$

$$P_{nl} = \begin{cases} P_{ne} & \text{for } \lambda_l \le 0.550 \\ \left[0.95 - 0.22\left(\frac{P_{crl}}{P_{ne}}\right)^{0.5}\right]\left(\frac{P_{crl}}{P_{ne}}\right)^{0.5} P_{ne} & \text{for } \lambda_l > 0.550 \end{cases} \tag{4}$$

In accordance with design rules codified in the ASCE/SEI 8-22 [9], the nominal axial strengths (P_{ASCE}) of the 13 CFSS built-up box section compression members were predicted and compared with their experimental ultimate capacities (P_{Exp}). As summarized in Table 3,

the mean value of P_{Exp}/P_{ASCE} equal to 0.89 with the corresponding COV of 0.128. Based on the resistance factor (ϕ) of 0.90, the reliability index (β) was calculated as 2.24, which is smaller than the target value of 2.5. It is revealed that the current DSM local buckling curve specified in the ASCE/SEI 8-22 [9] would result in unconservative and unreliable strength predictions for the cold-formed high-strength austenitic stainless steel built-up box section members under axial compression. This could be due to the semi-empirical nature of the DSM strength curve, which was calibrated against data on limited types of cross-sectional profiles excluding the built-up box-sections. Among the three types of built-up section configurations, the strength predictions (P_{ASCE}) of the UU-section stub columns were most unconservative, as demonstrated in Figure 8.

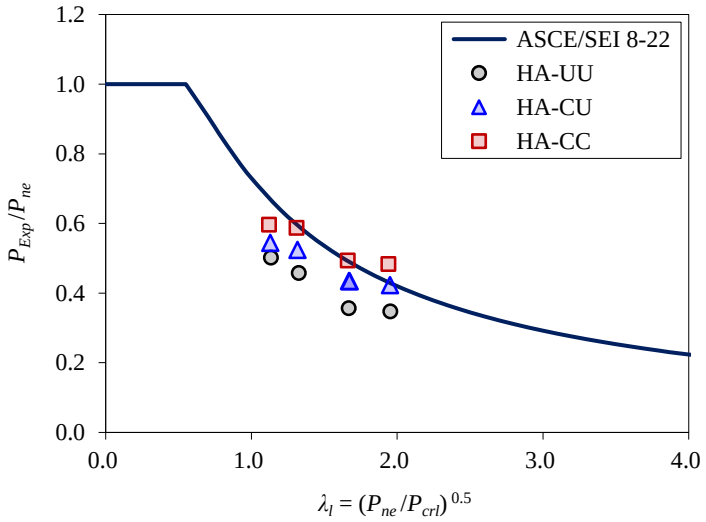

Figure 8: Comparison of experimental ultimate capacities with codified DSM curve.

4 CONCLUSIONS

The structural performance of cold-formed stainless steel built-up box section stub columns was experimentally investigated. The unlipped and lipped channels were brake-pressed from stainless steel thin sheets of high-strength austenitic grade QN1803 to assemble built-up section members using self-plugging rivets. Three built-up sectional configurations (i.e., UU-, CU- and CC-sections) with four nominal values of overall web height-to-plate thickness ratio (H_w/t) (i.e., 50, 60, 67 and 80) were considered in the test program. A total of 13 stub columns were tested to obtain failure modes, load versus axial shortening responses and ultimate capacities. It was found that the failure mode of the 13 stub column specimens was dominated by local buckling. Generally, the failure occurred near the mid-length of the specimens, where the webs and flanges of the built-up box sections buckled outward and inward, respectively. In addition, the results manifested that, for identical values of H_w/t ratio, the test specimens of UU- and CC-sections exhibited the smallest and greatest normalized loading capacities (P_{Exp}/P_y), respectively, which indicated that the built-up CC-sections consisting of two lipped channels outperformed in retarding local buckling than the UU-sections assembled by two unlipped channels. On the other hand, regarding the same built-up box sectional configurations, the normalized loading capacities (P_{Exp}/P_y) of the specimens generally decreased with the increase of H_w/t ratio. Furthermore, the experimental results were utilized to assess the suitability of design rules specified in the recently updated ASCE/SEI 8-22 [9] for cold-formed stainless steel built-up section members subjected to axial compression. It is shown that the DSM local buckling curve codified in the ASCE/SEI 8-22 specification [9] offered over-optimistic and

unreliable strength predictions for the cold-formed high-strength austenitic stainless steel built-up box section stub columns.

ACKNOWLEDGEMENTS

This research work was supported by a grant from the National Natural Science Foundation of China (Project No. 52008243). The authors are also grateful to Mr. Xin Huang, Mr. Cheng-Jian Shao and Ms. Miao Fu for their assistance in the test program.

REFERENCES

[1] Baddoo N.R., "Stainless steel in construction: A review of research, applications, challenges and opportunities", *Journal of Constructional Steel Research*, **64**, 1199-1206, 2008.

[2] Gardner L., "Stability and design of stainless steel structures – Review and outlook", *Thin-Walled Structures*, **141**, 208-216, 2019.

[3] Li H.-T. and Young B., "Behaviour of concrete-filled ferritic stainless steel tubular joints: Experimental investigation, numerical modelling and design", *Engineering Structures*, **247**, 113109, 2021.

[4] Meza F.J., Becque J. and Hajirasouliha I., "Experimental study of the cross-sectional capacity of cold-formed steel built-up columns", *Thin-Walled Structures*, **155**, 106958, 2020.

[5] Phan D.K., Rasmussen K.J.R. and Schafer B.W., "Tests and design of built-up section columns", *Journal of Constructional Steel Research*, **181**, 106619, 2021.

[6] Zhou T., Li Y., Ren L., Sang L. and Zhang L., "Research on the elastic buckling of composite webs in cold-formed steel back-to-back built-up columns – Part I: Experimental and numerical investigation", *Structures*, **30**, 115-133, 2021.

[7] Vy S.T. and Mahendran M., "Behaviour and design of slender built-up nested cold-formed steel compression members", *Engineering Structures*, **241**, 112446, 2021.

[8] Zhou X., Xiang Y., Shi Y., Xu L. and Zou Y., "Simplified design method of cold-formed steel columns with built-up box sections", *Engineering Structures*, **228**, 111532, 2021.

[9] ASCE, Specification for the design of cold-formed stainless steel structural members, *ASCE/SEI 8-22*, American Society of Civil Engineers and Structural Engineering Institute, Reston, USA, 2022.

[10] Zhou Y., Chouery K.E., Xie J.-Y., Shu Z. and Jia L.-J., "Full-range plasticity of novel high-performance low-cost stainless steel QN1803", *Steel and Composite Structures*, **35**(6), 739-752, 2020.

[11] ASTM, Standard test methods for tension testing of metallic materials, *ASTM E8/E8M-21*, American Society for Testing Materials, West Conshohocken, USA, 2022.

[12] Li H.-T. and Young B., "Cold-formed ferritic stainless steel tubular structural members subjected to concentrated bearing loads", *Engineering Structures*, **145**, 392-405, 2017.

[13] Li H.-T. and Young B., "Cold-formed stainless steel RHS members undergoing combined bending and web crippling: Testing, modelling and design", *Engineering Structures*, **250**, 113466, 2022.

[14] Li Q.-Y. and Young B., "Experimental and numerical investigation on cold-formed steel built-up section pin-ended columns", *Thin-Walled Structures*, **170**, 108444, 2022.

[15] Schafer B.W., Glauz R.S. and Chen H., "Revision of ASCE 8-Design of cold-formed stainless steel structural members", *Journal of Constructional Steel Research*, **208**, 107986, 2023.

[16] Arrayago I. and Rasmussen K.J.R., "Buckling curves for cold-formed stainless-steel columns and beams", *Journal of Structural Engineering*, **147**(10), 04021149, 2021.

[17] Becque J., Lecce M. and Rasmussen K.J.R., "The direct strength method for stainless steel compression members", *Journal of Constructional Steel Research*, **64**(11), 1231-1238, 2008.

[18] Schafer B.W. and Ádány S., "Buckling analysis of cold-formed steel members using CUFSM: conventional and constrained finite strip methods", *Proceedings of the 18th International Specialty Conference on Cold-Formed Steel Structures*, Orlando, Florida, USA, 2006.

[19] Li Z. and Schafer B.W., "Application of the finite strip method in cold-formed steel member design", *Journal of Constructional Steel Research*, **66**(8-9), 971-980, 2010.

[20] Li Q.-Y. and Young B., "Structural behaviour of cold-formed steel built-up closed section beam-columns", *Thin-Walled Structures*, **181**, 110087, 2022.

[21] Li Q.-Y. and Young B., "Numerical investigation and design of cold-formed steel built-up section beam-column members under moment gradients", *Engineering Structures*, **283**, 115746, 2023.